Syntheses, Crystal Structures, and Magnetic Properties of Metal-Organic Hybrid Materials of Mn(II)/Co(II): Three-fold Interpenetrated α-Polonium-like Network in One of Them

Soumen Mistri,[†] Subal Chandra Manna,[†,*] Ennio Zangrando,[‡] Albert Figuerola,[§] Joan Cano,[£,*] and Amit Adhikary [€]

[†]*Department of Chemistry and Chemical Technology, Vidyasagar University, Midnapore 721102, West Bengal, India, E-mail: scmanna@mail.vidyasagar.ac.in, Fax: (91) (03222) 275329.*

[‡]*Department of Chemical and Pharmaceutical Sciences, University of Trieste, 34127 Trieste, Italy.*

[§]*Department of Inorganic Chemistry and Nanoscience and Nanotechnology Institute (IN2UB), University of Barcelona, Martí i Franquès 1-11, 08028 Barcelona, Spain.*

[£]*Instituto de CienciaMolecular (ICMol) and Fundació General de la Universitat de València (FGUV), Universitat de València, E-46980 Paterna, València, Spain.*

[€] *Department of Chemistry, IISER Bhopal, Bhopal 462023, MP, India.*

ABSTRACT: Three new 1,4-phenylenediacrylate bridged Mn(II) and Co(II) complexes with the molecular formulae $\{[Mn_2(phen)_4(H_2O)_2(ppda)]\cdot(ppda)\cdot 2(H_2O)\}$(**1**), $\{[Co(ppda)(dpyo)(H_2O)_3]\cdot 4(H_2O)\}_n$ (**2**), and $\{[Co(ppda)(bpe)]\cdot(0.5H_2O)\}_n$ (**3**) [phen = 1,10-phenanthroline; ppda = 1,4-phenylenediacrylate; dpyo = 4,4´-dipyridyl *N,N´*-dioxide; bpe = 1,2-bis(4-pyridyl)ethane] have been synthesized and characterized by elemental analysis, IR spectra, single-crystal X-ray diffraction studies and low temperature magnetic measurements. Structural determination reveals that complex **1** is dinuclear, **2** is a 1D polymeric chain, while **3** is a three-fold interpenetrated α-polonium-like network. Hydrogen bonding interactions, formed by coordinated and/or lattice water molecules with ppda oxygen, and π–π staking interactions of aromatic rings lead to a 3D supramolecular architecture in both complexes **1** and **2**. Low

temperature magnetic study shows antiferromagnetic coupling in all the complexes. In addition, their electronic and fluorescent spectral properties have also been investigated.

INTRODUCTION

Metal-organic hybrid materials built from 3d metal ions and organic bridging ligands have become a very attractive research field for chemists due to their intriguing structural diversity based on supramolecular assemblies[1] and potential applications as functional materials in fields of catalysis, porosity, magnetism, luminescence, conductivity, sensing, nonlinear optics and chirality.[2-7] The compositional / structural diversities of metal-organic hybrid materials may be tuned by a suitable choice of ligands as well as of metal ions, because the variation of molecular size, symmetry, substituent group and backbone flexibility of organic linkers can result in materials having diverse architectures and functions. A literature survey shows that the most commonly used strategies for the synthesis of metal-organic hybrid materials are the use of (a) anionic bridging ligands, which, in addition, can partially or fully counterbalance the charge of the metal centers, (b) anionic as well as neutral spacers to increase the possibility of enhancing the dimensionality of compounds, and (c) only neutral spacers, where charges of the metal centers are counterbalanced by non-coordinating anions. Bi or multi dentate ligands containing N or / and O-donors are usually employed to bind metal centres and various architectures e.g. diamondoid,[8] honeycomb,[9] grid[10] T-shaped,[11] ladder,[12,13] brick wall[10a,12] and octahedral[14] have been repeated by suitable combination of spacers. The use of long spacers (rigid/flexible)[15] in the quest of porous materials often yields to interpenetrated networks with reduced/no void space, with a few exceptions where substantial amount of void space persists even after

interpenetration.[16] The appearance of interpenetration is due to the natural tendency of molecular building blocks to pack most efficiently in the crystalline state. A large number of interpenetrated networks have been found from 2-fold to even beyond 10-fold.[17] It is interesting to note that the interpenetration between the same networks is very common because the same molecular fragments favor the same periodicity.[18]

Di or poly-carboxylates have also been used to form robust frameworks, since in this case functional groups exhibit a variety of coordination modes. Several groups as well as our lab reported the synthesis and characterization of a large number of carboxylato bridged multidimensional architectures in presence of nitrogen/oxygen donor co/bridging neutral ligands.[19,20] *p*-Phenylediacrylic acid (H_2ppda), as a member of multidentate aromatic polycarboxylic acid, possesses special conformations with a 180° angle between the carboxylic groups and versatile coordination modes (Chart **1**). It has been scarcely used to construct coordination polymers,[21] although it can function as mediator for transmitting the exchange interaction between paramagnetic metal centers.[21a] To our knowledge, only a few compounds of ppda have been reported in the literature. The transition metals ions are often used in syntheses based on the interest of their magnetic properties. It is interesting to note that several 3D metal-organic hybrid materials have shown long-range magnetic ordering with values of the critical temperature (T_c) up to 70 K.[22] Recently several papers have confirmed that highly anisotropic Co(II) ions can show slow magnetic relaxation dynamics that lead to the preparation of Single Ion Magnets, which have potential applications in molecular spintronics, ultra-high density magnetic information storage, and quantum computing at the molecular level.[23] On the other hand, isotropic Mn(II) was also used for simplicity and easy understanding of the magnetic coupling established through the $ppda^{2-}$ ligand and its multidentate nature offers the possibility to

grow higher dimensional metal-organic frameworks with tunable magnetic properties depending on the coordination geometry of the complex. So it is important to study the potential and versatility of this linker both in terms of coordination chemistry and magnetic exchange mediator.

In this contribution, ppda was employed to synthesize three novel coordination compounds, namely $\{[Mn_2(phen)_4(H_2O)_2(ppda)]\cdot(ppda)\cdot 2(H_2O)\}$(**1**), $\{[Co(ppda)(dpyo)(H_2O)_3]\cdot 4(H_2O)\}_n$ (**2**), and $\{[Co(ppda)(bpe)]\cdot(0.5H_2O)\}_n$ (**3**) [phen = 1,10-phenanthroline; ppda = 1,4-phenylenediacrylate; dpyo = 4,4´-dipyridyl *N*,*N*´-dioxide; bpe = 1,2-bis(4-pyridyl)ethane]. These compounds exhibit diverse structural dimensions: **1** is a discrete dinuclear complex, **2** is a 1D coordination polymer, while **3** is a 3D three-fold interpenetrated α-polonium-like network. Hydrogen bonding and π–π staking interactions of aromatic rings lead to a 3D supramolecular architecture in both complexes **1** and **2**.

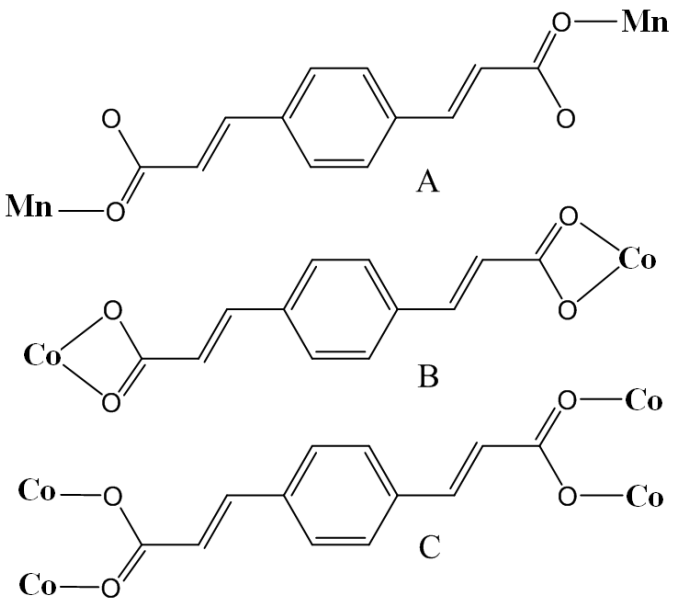

Chart 1: Coordination mode of ppda in the present complexes: A) *bis*-monodentate ($\eta^2\mu$in **1** and **2**), B) chelating *bis*-bidentate$\eta^4\mu$and C) bridging tetra-monodentate$\eta^4\mu_2$:$\mu_2$in **3**.

EXPERIMENTAL SECTION

Materials. High purity 1,2-bis(4-pyridyl)ethane (bpe) (98%), 1,4-phenylenediacrylic acid (H_2ppda) (97%), 4,4´-dipyridyl *N*,*N*´-dioxide (dpyo), 1,10-phenanthroline monohydrate and manganese(II) chloride tetrahydrate (98%) were purchased from the Aldrich Chemical Co. Inc. and were used. All other chemicals were of AR grade.

Physical Measurements. Elemental analyses (carbon, hydrogen and nitrogen) were performed using a Perkin-Elmer 240C elemental analyzer. IR spectra were recorded as KBr pellets on a Bruker Vector 22FT IR spectrophotometer operating from 400 to 4000 cm^{-1}. The UV/Vis reflectance spectra were recorded between 200–1400 nm on a UV-3600, Shimadzu UV-vis-NIR spectrophotometer at room temperature in the solid state. $BaSO_4$ powder was used as standard (baseline). Emission spectra were recorded on a Hitachi F-7000 spectrofluorimeter at room temperature.

Synthesis of {[Mn_2(phen)$_4$(H_2O)$_2$(ppda)]·(ppda)·2(H_2O)}(1). A methanolic solution (10 mL) of manganese(II) chloride tetrahydrate (1 mmol, 0.197 g) was allowed to react with a methanolic solution (10 mL) of 1,10-phenanthroline monohydrate (1 mmol; 0.198 g) and stirred for 15 min. Then, an aqueous solution (20 mL) of disodium 1,4-phenylenediacrylate (Na_2ppda) (1mmol, 0.262 g) was poured slowly into it and the resulting mixture was refluxed for 4 h. It was then allowed to cool and filtered. The filtrate was kept in air for slow evaporation and yellow colored single crystals suitable for X-ray diffraction were obtained after a few days. Yield 1.028 g (75%). $C_{72}H_{60}Mn_2N_8O_{14}$ (1371.16): C, 63.01; H, 4.37; N, 8.16%. Found: C, 63.59; H, 4.38; N, 8.15 (%). IR (cm^{-1}): 3491(w), 3358(w), 3050(w), 1707(s), 1636(s), 1563(s), 1513(s), 1423(vs),

1372(vw), 1288(w), 1257(vw), 1144(w), 1102(w), 979(s), 856(w), 838(s), 784(vw), 768(vw), 728(s), 703(w), 635(w), 544(w), 507(vw), 419(vw).

Synthesis of {[Co(ppda)(dpyo)(H_2O)$_3$]·4(H_2O)}$_n$ (2). A methanolic solution (5 mL) of 4,4´-dipyridyl *N*,*N*´-dioxide (dpyo) (1 mmol, 0.188 g) was added dropwise to a methanolic solution (5 mL) of $CoCl_2·6H_2O$ (1 mmol, 0.291 g) with constant stirring. An aqueous solution (10 mL) of disodium 1,4-phenylenediacrylate (Na_2ppda) (1mmol, 0.262 g) was added to the resulting light-red reaction mixture and stirred for 3 h. A deep-red complex separated out. Single crystals suitable for X-ray analysis were obtained by diffusing a methanolic solution (10 mL) of dpyo and $CoCl_2·6H_2O$ (1:1) mixture into an aqueous (10 mL) layer containing disodium 1,4-phenylenediacrylate (Na_2ppda) in a tube. Deep-pink crystals deposited at the junction of the two layers after a few days. Yield: 0.471 g (80 %). Anal. Calcd for $C_{22}H_{30}CoN_2O_{13}$(589.41): C, 44.79; H, 5.08; N, 4.75 (%). Found: C, 44.77; H, 5.10; N, 4.73(%). IR (cm^{-1}): 3453(w), 3344(w), 3015(vw) , 1638(s), 1537(s), 1418(w), 1389(s), 1295(vw), 1259(w), 1195(vw), 1113(vw), 984(vs), 888(w), 837(s), 741(vw), 699(w), 550(vw), 512(w).

Synthesis of {[Co(ppda)(bpe)]·(0.5H_2O)}$_n$ (3). The complex was synthesized following the same procedure adopted for complex **2**using 1,2-bis(4-pyridyl)ethane (bpe) (1 mmol, 0.184 g) instead of dpyo. Single crystals suitable for X-ray analysis were obtained by diffusing a methanolic solution (10 mL) of bpe and $CoCl_2·6H_2O$ (1:1) mixture into an aqueous (10 mL) layer containing disodium 1,4-phenylenediacrylate (Na_2ppda) in a tube. Deep-red crystals deposited at the junction of the two layers after a few days. Yield: 0.365 g (78 %). Anal. Calcd for $C_{24}H_{21}CoN_2O_{4.50}$ (468.36): C, 61.49; H, 4.48; N, 5.97 (%). Found: C, 61.47; H, 4.50; N, 5.96(%).IR (cm^{-1}): 3000-3500(br,s), 1641(s), 1612(s), 1583(w), 1564(w), 1541(w), 1509(w),

1426(vs), 1393(vs), 1289(w), 1259(w), 1114(w), 1071(w), 1018(w), 983(s), 881(w), 830(s), 721(w), 695(w), 548(w), 507(vw).

Crystallographic Data Collection and Refinement.

Data collections for complexes **1**,**2**, and**3**were carried out at room temperature with Mo-Kα radiation (λ = 0.71073 Å) on a Bruker Smart Apex diffractometer equipped with CCD. Cell refinement, indexing and scaling of the data sets were done by using programs Bruker Smart Apex and Bruker Saint packages.[24] The structure was solved by direct methods and subsequent Fourier analyses[25] and refined by the full-matrix least-squares method based on F^2 with all observed reflections.[25] On the ΔFourier map of **3** a ppda anion and one py ring of the bpe were found disordered: the former is located about a center of symmetry (occupancy 0.5), the second due to rotational disorder was refined over two positions with occupancies refined at 0.506(8)/0.494(8). Hydrogen atoms were placed at calculated positions, those of lattice water molecules were located on the ΔFourier map and refined. A residual in complex **3** was successfully refined as a water oxygen at half occupancy (H atoms not located) All the calculations were performed using the WinGX System, Ver 1.80.05.[26] Crystal data and details of refinements are given in Table 1.

Magnetic Measurements.

Temperature-dependent molar susceptibility measurements of polycrystalline samples of **1 - 3** were carried out at the ‘‘Servei de Magnetoquímica (Universitat de Barcelona)’’ in a Quantum Design SQUID MPMSXL susceptometer with an applied field of 3000 and 198 G in the temperature ranges 2–300 and 2–30 K, respectively. For 3, molecular susceptibility measurements were also done at 10000, 5000, 100 and 50 G in the temperature range 2–300 K.

Magnetization curves were collected for 2 between 2 and 10K in the magnetic field range 0–5000 G.

RESULTS AND DISCUSSION

IR Spectral Studies.

The most important absorption bands in IR spectroscopy of complexes under study are summarized in experimental section and tabulated in Table 1S. The spectra (Figures 1S-3S) of complexes **1**, **2** and **3** exhibit bands at 1636, 1638 and 1641 cm^{-1}, respectively, corresponding to ν_{as}(OCO), while the ν_s(OCO) appears at 1423, 1418 and 1426 cm^{-1}, respectively. Aromatic ν(C=C, C=N) stretching vibrations for **1**, **2** and **3** appear in the region 1513-1563 cm^{-1}, 1537 cm^{-1} and 1509-1612 cm^{-1}, respectively. The bands in the region 3015-3050 cm^{-1} corresponds to the aromatic ν(C-H) stretching vibrations. The spectra of complexes **1**, **2** and **3** show broad bands in the region 3100-3550 cm^{-1}, which are assigned to the ν(O–H) stretching vibrations of water molecules.[27] For **3**, band at 2910 cm^{-1} is due to the $\nu(C–H)_{aliphatic}$ stretching vibration. The bands at 1195 and 837 cm^{-1} corresponds to ν(N-O) and δ(N-O) vibration, respectively, for **2**.The IR spectra of **1** and **2** also show bands corresponding to $\rho_r(H_2O)$ [at 768 cm^{-1} for **1**, 741 cm^{-1} for **2**] and to $\rho_w(H_2O)$ [at 544 cm^{-1} for **1**, 550 cm^{-1} for **2**] indicating the presence of coordinated water molecules.

Electronic Spectra and Luminescent Properties.

The solid state reflectance spectra of all the complexes have been recorded (Figure 4S), and the data were collected in Table 2S. For complex **1** no characteristic spin allowed d-d electronic

transitions are observed in the electronic spectra. This is due to the fact that for Mn(II) high spin complex the ground state is ^{6}S, which is orbitally non-degenerate and cannot split by a crystal field of any symmetry. The absence of any other spin sextet term implies that all the crystal field transitions from the ^{6}S will be spin forbidden, as well as Laporte forbidden. A series of bands in the region 23148 – 33003 cm^{-1} can be assigned to spin forbidden transition to spin quartets [$\bar{\nu}$, 23148 cm^{-1}; λ, 432 nm for $^6A_{1g}$ (S)→$^4T_{2g}$(G); $\bar{\nu}$, 25000 cm^{-1}; λ, 400 nm for$^6A_{1g}$(S) → $^4A_{1g}$(G); $\bar{\nu}$, 25252 cm^{-1}; λ, 396 nm for $^6A_{1g}$(S) → ^4E_g(G); $\bar{\nu}$, 29761 cm^{-1}; λ, 336 nm for$^6A_{1g}$ (S) → ^4E_g(D) and $\bar{\nu}$, 33003 cm^{-1}; λ, 303 nm for$^6A_{1g}$ (S)→$^4T_{1g}$(P)]along with intra ligand charge transfer transitions of organic ligand.[28] For complexes **1** and **2**,the band in the region 8382- 8568.98 cm^{-1} ($\bar{\nu}$, 8382 cm^{-1}; λ, 1193 nm for **2** and $\bar{\nu}$, 8568 cm^{-1}; λ, 1167 nm for **3**) can be assigned to the spin allowed d-d transition $^4T_{1g}$(F)→$^4T_{2g}$(F). In addition a multiple band, observed in the visible region at 514 nm (19455 cm^{-1}) and 491 nm (20366 cm^{-1}) for **2** and **3**, respectively, can be assigned to another spin allowed d-d transition $^4T_{1g}$(F)→$^4T_{1g}$(P) admixed with spin forbidden transition to doublet state derived principally from the free ion ^{2}G and ^{2}H terms.[28] A very weak band ($\bar{\nu}_2$), 620 nm (16129 cm^{-1}) and 617 nm (16207 cm^{-1}) for **2** and **3** respectively, corresponds to the spin allowed $^4T_{1g}$(F)→$^4A_{2g}$(F) transition. From the Orgel diagram (ignoring configuration interaction) for weak field octahedral cobalt(II) (d^7) compounds it is clear that $\bar{\nu_1}$ = 8Dq, $\bar{\nu_2}$ = 18 Dq and $\bar{\nu_3}$ = 6Dq+15B. This relation allowed calculating the 10 Dq and B values for the two compounds. The former values (10 Dq) of 7746 and 7638 cm^{-1} for **2** and **3**, respectively, (Table 2S) indicate that the ligand field strength for **2** is relatively higher with respect to that of **3**. Calculated B values are 987 and 1052 cm^{-1} for **2** and **3**, respectively.

The emission spectra of complexes **1**, **2** and **3** in solid state at room temperature are depicted in Figure 1. It can be observed that intense emissions occur at 394 and 467 nm (λ_{ex}=

270 nm) for **1**, 465 nm (λ_{ex} = 275 nm) for **2** and 415 nm (λ_{ex} = 300 nm) for **3**. These emissions may be assigned as intra ligand charge transfer (ILCT) of the neutral N/O donor ligands.[29]

Crystal Structure Description.

[Mn$_2$(phen)$_4$(H$_2$O)$_2$(ppda)]·(ppda)·2(H$_2$O)(1). The crystal structure of complex **1** consists of discrete dinuclear $[Mn_2(phen)_4(H_2O)_2(ppda)]^+$ cations, ppda anions and lattice water molecules. The centro-symmetrical complex cation, shown in Figure 2, comprises two $[Mn(phen)_2(H_2O)]$ units connected by a ppda in a bis-monodentate fashion spacing the metals by 15.594 Å. The manganese atom presents a highly distorted octahedral geometry with Mn-N bond lengths in a range 2.295(3)-2.305(3) Å, while the Mn-O bonds are somewhat shorter of 2.119(2) and 2.126(2) Å (Table 2). These values are close comparable to those found in the 1D polymer $[Mn(ppda)(phen)(H_2O)_2]$.[30] In the present complex the occurrence of a second phen ligand in the metal sphere hampers the formation of a coordination polymeric species. The phenanthroline ligands coordinate the Mn atom with a chelating angle of ca 72° and are arranged so that their mean planes make a dihedral angle of 66.20(5)°. The aqua ligand forms H-bonds with carboxylate groups of two uncoordinated ppda rather to form an intra-molecular H-bond with the adjacent carboxylate oxygen O(2).

The crystal packing reveals the formation of π-π stacking interactions among aromatic rings of the py rings and dppa in addition of H-bonds due to the numerous water molecules. As far as aromatic rings interactions, both phen ligands are involved: the N3,N4-phenanthrolines of symmetry related complexes sandwich the uncoordinated ppda (centroid-to-centroid distances of 3.756(3) Å) as shown in Figure 3. Moreover the N3,N4-phen ligand faces a symmetry related

one (centroid-to centroid distances of 3.599(4) Å), and the N1-pyridine of each complex is faced to the central ring of the N1,N2-phen of a symmetry related complex at a distance of 3.655(2) Å as shown in Figure 4. All these interactions give rise to a 3D network arrangement. In addition the aqua ligand O(1w) and the two lattice water molecules are involved in the formation of a H-bonding scheme with dppa oxygens. The structural parameters of these interactions are reported in Table 3.

*{[Co(ppda)(dpyo)(H_2O)$_3$]·4(H_2O)}$_n$(**2**).* The X-ray structural analysis of complex **2** revealed that it is a 1D polymeric chain –[Co1–ppda–Co2–ppda]$_n$– comprising of two independent cobalt ions, having an O_6 donor set in an octahedral centro-symmetric environment and linked by the bis-monodentate ppda anions at a distance of 16.132 Å (Figure 5). The metal ion Co(1) is coordinated by four aqua ligands and two oxygens from different ppda, while Co(2) has two water molecules, two oxygens from ppda and completes the coordination sphere by two oxygen donors from different dipyridyl dioxide molecules. The latter ligands result to be monodentate and pendant from the polymeric array. The selected bond distances and angles reported in Table 2 indicate that the Co-O bond lengths fall in a range from 2.0375(14) to 2.1564(18) Å, the longest value being relative to the Co(2)-O(3w) bond distance. However it is not obvious to correlate the variation of these Co-Ow values with the H-bonds formed by the aqua ligands (see below). The polymeric array is reinforced by rather strong intra molecular H-bonds, occurring between the coordinated water molecules and adjacent carboxylate O atoms, the O(1w)…O(4) and O(2w)…O(6) distances being of 2.676 and 2.690 Å, respectively. The dpyo ligand, connected to the metal with a N(1)-O(1)-Co(1) angle of 120.18(11), is tilted by ca 32° with respect to the direction of the polymer propagation. Symmetry related polymers are piled and connected through strong π-π stacking interactions between the dpyo pyridine and the ppda

phenyl rings (centroid-to-centroid distance is 3.4900(14) Å) to give rise to a 2D layer parallel to the crystallographic [102] planes (Figure 6). In addition the layered architecture is reinforced by H-bonds between the coordinated water O(3w) and oxygen O(2) of the terminal dpyo molecule. A 3D architecture is finally obtained through a H-bonding scheme involving the coordinated aqua ligands and the lattice water molecules (Table 3).

*{[Co(ppda)(bpe)].(0.5H_2O)}$_n$(**3**).* The asymmetric unit of complex **3** contains a cobalt ion, a bpe ligand and two half ppda anions. A residual in the ΔFourier map was assigned to lattice water oxygen of half occupancy. As shown in Figure 7 the cobalt ion is octahedrally coordinated by two nitrogen atoms of two bpe ligands and four oxygen atoms from three ppda anions. Both the independent ppda anions are hinged on inversion centres and thus symmetrically connect the cobalt atoms in two coordination modes: one bridges four Co atoms with carboxylate groups in a *syn-syn* fashion ($\eta^4\mu_2$:μ_2), the other acts as bis-chelating ($\eta^4\mu$) towards two Co atoms (Chart 1). In the former case an eight-membered ring $[Co(COO)]_2$ is formed, where the metals are separated by 4.3395(12) Å. The Co-O distances relative to the chelating carboxylates are slightly longer (Co-O(3) = 2.173(3), Co-O(4) = 2.201(3) Å) with respect to those of bridging groups (Co-O(1) = 1.994(3) Co-O(2') = 2.021(3) Å), while the Co-N bond lengths of 2.165(3) and 2.152(4) Å are comparable within their esd (Table 2). The measured intermetallic distance within the eight-membered ring $[Co(COO)]_2$ is comparable with the values of 4.00-4.40 Å detected in structures comprising similar binuclear nodes.[31] These distances appear to be modulated by the different ligands used and ultimately by packing forces.

The structure of the present compound consists of rectangular sheet of dimensions of 19.70 x 14.74 Å, as shown in Figure 8, where the binuclear Co_2 subunits are inter-connected through ppda ligands. The sheets are further parallel aligned and linked by bpe spacers to

generate an infinite three-dimensional co-ordination framework featuring cuboidal structural units as shown in Figure 9. The structure is a three-fold interpenetrated α-polonium-like network,[32] in which the binuclear Co nodes are linked together by three different types of rods: bis-bridging ppda, bis-chelating ppda, and double bpe connectors, which spaces the nodes (middle point of Co_2 units) at different distances, namely 14.745(2), 19.704(3), and 13.581(2) Å, respectively. Figure 10 illustrates a simplified scheme of the three interpenetrated network with indication of the eight-membered rings and carboxylates. Similar coordinated frameworks of formulation [M(tp)(4,4´-bipy)] (M = Co, Cd, Zn, tp = terephthalate; 4,4´-bipy = 4,4´-bipyridine), which present a two-fold interpenetration network, have been already reported a decade ago.[33] Interestingly the use of longer N,N´-donor ligand and dicarboxylate anion as connectors in **3**, led to a comparable architecture but the order of interpenetration is increased to three-fold. Moreover since the effective free volume of **3** was calculated by Platon analysis[34] as 12.0% of the crystal volume (142.4 out of the 1190.6 $Å^3$ unit cell volume), the three fold interpenetrated structure, when viewed down axis-*a*, draws channels which are occupied by disordered lattice water molecules H-bonded to the ppda (Figure 8).

Magnetic Properties.

Complex 1. Temperature-dependent magnetic susceptibility measurements on a polycrystalline sample of complex **1** were carried out with an applied field of 0.3 T in the temperature range 1.9-300 K. The plot of $\chi_M T$ versus T is shown in Figure 11, where χ_M is the molar magnetic susceptibility and T is the absolute temperature. The $\chi_M T$ value measured at room temperature, of 8.48 $cm^3\ mol^{-1}$ K, roughly matches the expected value of 8.74 $cm^3\ mol^{-1}$ K obtained from the sum of two Mn(II) ions. Upon cooling, $\chi_M T$ keeps constant until a temperature of 50 K. Below

this temperature the $\chi_M T$ versus T curve starts decreasing until a $\chi_M T$ value of 8.12 cm^3 mol^{-1} K is reached. The behavior displayed by complex **1** suggests the presence of an overall antiferromagnetic interaction between the Mn(II) ions in the dinuclear unit. In order to quantitatively interpret these data, a simulation was performed with the MAGPACK program in an attempt to reproduce the experimental curve.[35] In this model, the crystallographic equivalence of the two Mn(II) ions in the dinuclear unit was considered by assigning one single g value for that ion. For the spin Hamiltonian $H= -JS_1S_2$, $S_1= S_2= S_{Mn}$, a good agreement between the experimental and simulated curves for **1** was found by using the following parameters: $g_{Mn}= 1.97$ and $J_{Mn\text{-}Mn} = -0.02$ cm^{-1}. The simulated curve is represented together with the experimental values in Figure 11.

Complex 2. The magnetic properties of **2** under the form of $\chi_M T$ versus T plot [χ_M is the magnetic susceptibility per Co(II) ion] are shown in Figure 12. $\chi_M T$ at room temperature is equal to 2.58 cm^3 mol^{-1} K, a value that is larger than the expected one for the spin-only case ($\chi_M T$ = 1.875 cm^3 mol^{-1} K with S_{Co} = 3/2 and g_{Co} = 2.0). This fact indicates that the distortion of the octahedral symmetry of Co(II) in **2** is not so large to induce the total quenching of the $^4T_{1g}$ ground state.[36] Upon cooling, initially $\chi_M T$ decreases smoothly and later faster. Below 50 K, $\chi_M T$ shows a tendency that would lead to a non-zero value at 0 K (around 1.6 cm^3 mol^{-1} K). However, below 20 K the $\chi_M T$ abruptly decreases reaching a value of 1.14 cm^3 mol^{-1} K at 2.0 K, but no maximum is observed in the magnetic susceptibility in the temperature range explored. The decrease of the $\chi_M T$ in the high temperature region is due to the progressive depopulation of the high-energy Kramers doublets (spin-orbit coupling effects), as expected for six coordinated high-spin cobalt(II) complexes.[36] This interpretation is supported by the fact that the value of $\chi_M T$ at 20 K and that expected at 0 K from the followed trend at high temperatures [1.92 cm^3 mol^{-1} K

and 1.6 cm^3 mol^{-1} K, respectively] is well above in one case or close in the other to that calculated for a magnetically isolated cobalt(II) ion (1.73 cm^3 mol^{-1} K for a Seff = 1/2 with g ≈ 4.3). The decrease of $\chi_M T$ below 20 K, which takes values lower than that calculated for a magnetically isolated cobalt(II) ion, can be interpreted as due to an overall weak antiferromagnetic coupling between the Co(II) ions through the L extended ligand. The magnetic susceptibility data for **2** were analyzed in the region T > 30 K by introducing SOC effects through the Hamiltonian: $\widehat{H} = \alpha\lambda\hat{L}\cdot\hat{S} + \Delta\left[\hat{L}_z^2 - \hat{L}\left(\hat{L}+1\right)/3\right] + \delta\left(\hat{L}_x^2 - \hat{L}_y^2\right) + \beta H \cdot \left(-\alpha\hat{L} + g_e\hat{S}\right)$ where λ is the spin-orbit coupling parameter, α is the orbital reduction factor, and Δ is the axial orbital splitting of the T_1 term.[36] Using the VPMAG package,[37] the best-fit (dashed line in Figure 12) was found with the values λ = –145 cm^{-1}, α = 1.271 and Δ = 967 cm^{-1}, with an agreement factor F of 2.0*10^{-5}, defined as $F = \sum\left[(\chi_M T)_{exp} - (\chi_M T)_{calc}\right]^2 / \sum\left[(\chi_M T)_{exp}\right]^2$. However, this model is not able to reproduce the experimental data below 20 K, which have been interpreted including a magnetic interaction between neighboring Co(II) ions. Thus, the system can be studied as a regular S = ½ chain with effective g factor and magnetic coupling. The effective g value at each temperature is obtained from the $\chi_M T$ value of a Co(II) ion extrapolated from the SOC Hamiltonian discussed above, while the effective magnetic coupling constant is expressed as J_{eff} = 25/9 J, being J the true magnetic coupling between two S = 3/2 Co^{II} ions.[36] This methodology was extensively described in a precedent paper.[33] A weak antiferromagnetic interaction between Co(II) ions is expected because its influence on the magnetic behavior is only observable at very low temperatures. In such case, it is also possible to use a regular ring model of S = 1/2 centers to simulate the experimental behavior. When magnetic interaction is stronger, the data at lower temperatures are poorer described and a higher temperature threshold is expected. Evidently, smaller ring models restrict fast the temperature region in which magnetic

behavior can be correctly simulated. In this case, it is possible to simplify the study using a ring model with ten centers that is large enough to process the experimental data of **2** and that can be done automatically with VPMAG code including the spin-orbit coupling phenomenon and the effective interaction Hamiltonian. The best-fit (solid line in Figure 12) was found with the values λ = –130 cm^{-1}, α = 1.341, Δ = 1007 cm^{-1} and J = –0.3 cm^{-1}, with an agreement factor F = 8.5*10^{-5}. On the other hand, when Δ is large enough and positive, as in this case, only the two lowest Kramers doublets, arising from the $^4A_2$ ground term, are thermally populated and the energy gap between them can be considered as an axial zero-field splitting (ZFS) within the quartet state with a positive D value.[36, 39, 40] Therefore the magnetic behaviour can be analysed by using the Hamiltonian $\boldsymbol{H} = D[\boldsymbol{S}_z^2 - S(S+1)/3] + E(\boldsymbol{S}_x^2 - \boldsymbol{S}_y^2) + g\mu_B H\boldsymbol{S}$, where S is the spin ground state, D and E are the axial and transverse magnetic anisotropies, respectively, μ_B is the Bohr magneton and H the applied magnetic field. The isothermal M vs. H/T plots (Figure 13) for **2** are not superimposed on a single master curve, being a clear evidence of the presence of significant magnetic anisotropy. Since the antiferromagnetic coupling in **2** is slightly affected by the temperature interval in which the magnetization data have been collected an easy and simultaneous analysis of the susceptibility and magnetization data cannot be performed, as previously done in other cases.[39] Thus, only susceptibility data at T > 30 K was analysed with this model. The values of parameters providing the best-fit were: g = 2.298 cm^{-1}, D = +46.5 cm^{-1}, E = –2.1 cm^{-1}, and TIP = 3.4*10^{-4} cm^3 mol^{-1}, with an agreement factor F = 4.5*10^{-6}. Similar values were found from a fit until 2 K which included a magnetic interaction along a regular chain of effective spin ½. These values were: g = 2.376 cm^{-1}, D = +49.6 cm^{-1}, E = –1.4 cm^{-1}, and J = –0.38 cm^{-1}, with an agreement factor F = 1.2*10^{-4}. In agreement with the previous best-

fit from and spin-orbit coupling model, a similar weak antiferromagnetic interaction between Co^{II} ions was found.

Complex 3. The $\chi_M T$ versus T plot of **3** [χ_M is the magnetic susceptibility per Co(II) ion] is shown in Figure 14. Likewise in **2**, χ_MT at room temperature (2.61 cm^3 mol^{-1} K) is larger than the expected one for the spin-only case. The $\chi_M T$ values decrease faster with decreasing temperature until an abrupt decrease is observed below 10 K. Thus, spin-orbit coupling affects the behavior of compound **3** and weak antiferromagnetic couplings are observed. From Figures 12 and 13, it seems that the magnetic couplings are weaker in **3**, probably, because of the less planarity in some of the extended ligands involved in the magnetic connection of the Co^{II} ions. However, an unexpected, sharp, and irregular increase of $\chi_M T$ around 60 K is observed. After it, a maximum of $\chi_M T$ (5.07 cm^3 mol^{-1} K with an applied magnetic field equal to 100 G) is reached at 43 K. This behavior, which is typical of a magnetic order, is dependent on the applied magnetic field (Figure 14) but only in the intermediate temperature region, i.e. below 5 K and above 60 K, the measured $\chi_M T$ values in presence of several magnetic fields are superimposed. Moreover, this maximum diminishes significantly in presence of higher magnetic fields and the recorded signals are very weak, which allows to conclude that this unusual behavior corresponds to the presence of a magnetic impurity which is magnetically ordered below 60 K. The co-precipitation of several phases of cobalt(II) hydroxides that show this kind of magnetic order is a usual phenomenon in the synthesis of such type of coordination compounds.[41] Several attempts to remove these impurities were done but they were all unsuccessful. Unfortunately, under such circumstances, it was not possible to analyze the magnetic behavior of **3** similarly as performed for complex **2**.

With regard to other compounds reported in literature with structural analogies with complexes 1-3, few of these systems have been magnetically studied so far, especially for what concerns Co(II) complexes. Usually either no magnetic study is performed or alternatively the magnetic behavior is interpreted by using the Curie-Weiss law where no single-ion effects from Co(II) are considered. [Jian-Qiang Liu, Yun-Sheng Huang, Ying-Yong Zhao, Zhen-Bin Jia, *Cryst. Gr. Des.* **2011**, *11*, 569-574] Just in a few cases some authors have used the same approach applied in our paper, [Qian Sun, Ai-ling Cheng, Yan-Qin Wang, Yu Ma, En-Qing Gao, *Inorg. Chem.* **2011**, *50*, 8144–8152; Xue-Hui Jing, Xiu-Chun Yi, En-Qing Gao, Vladislav A. Blatov, *Dalton Trans.*, **2012**, *41*, 14316-14328] as it was described for the first time by Lloret et al. [G. de. Munno, M. Julve, F. Lloret, J. Faus and A. Canneschi, *J. Chem. Soc., Dalton Trans.* **1994**, 1175; Francesc Lloret, Miguel Julve, Joan Cano, Rafael Ruiz-García, Emilio Pardo, *Inorg. Chim. Acta* **2008**, *361*, 3432–3445] However, even in these cases, the structural differences among the reported compounds and the presence of unquenched spin-orbit coupling in octahedral Co(II) coordination complexes make it difficult to extract further conclusions or magnetostructural correlations with current available tools. Nevertheless, the analysis of the magnetic behavior of similar compounds where paramagnetic ions are bridged by long carboxylato-based ligands like those used in complexes 1-3, show similar trends with respect to our systems: as observed in complex 1, where no spin-orbit is present, the exchange interaction between Mn(II) ions is very weak, and the same trend is observed for complexes 1 and 3 and those in literature, since the shortest metal-metal distances trough these ligands is above 13 Å and thus the bridge does not effectively transmit the exchange. [Qian Sun, Qi Yue, Jian-Yong Zhang, Li Wang, Xue Li, and En-Qing Gao, *Cryst. Gr. Des.* **2009**, *9*, 2310-2317;] In the specific case of complex 3, where two Co(II) ions are linked by two *syn-syn* carboxylate groups, also a weak antiferromagnetic exchange has been observed between them in agreement with the weak $J_{Co\text{-}Co}$ constants that can be found in the literature for multiple carboxylato-bridged Co(II) complexes. [Lu-Fang Ma, Li-Ya Wang, Yao-Yu Wang, Stuart R. Batten, Jian-Ge Wang, *Inorg. Chem.* **2009**, *48*, 915-924; Sanjit Konar, Ennio Zangrando, Michael G. B. Drew, Joan Ribas, Nirmalendu Ray Chaudhuri, *Dalton Trans. 2004*, 260-266]

CONCLUSION

In summary we have presented here the synthesis, crystal structure and low temperature magnetic behavior of three novel 1,4-phenylenediacrylate (ppda) bridged complexes of manganese(II) / cobalt(II) using N,N´- and O,O´ donor neutral ligand. Manganese(II)–ppda in combination with chelating phen ligand(**1**) and cobalt(II)-ppda with rigid rod like dpyo ligand (**2**) generates discrete dinuclear complexes, and 1D polymeric chain, respectively. Both **1** and **2** extend to 3D supramolecular architectures through H-bonding and π–π interactions. In both of

them ppda shows a *bis*-monodentate binding mode. On the other hand, a novel 3D interpenetrated α-polonium-like architecture is obtained by using long flexible connectors 1,2-bis(4-pyridyl)ethane in combination with ppda (**3**). Low temperature magnetic study reveals weak antiferromagnetic coupling in all the complexes.

ACKNOWLEDGEMENTS

Authors gratefully acknowledge the financial assistance given by the DST, Govt. of India, under the SERB Fast Track Scheme to Dr. Subal Chandra Manna (Grant No. SR/FT/CS-131 /2010). A.F. acknowledges financial support from the Spanish MINECO through CTQ2012-32247 and for a Ramón y Cajal Fellowship (RYC-2010-05821). J.C. acknowledges financial support from the Spanish Ministerio de Educación y Ciencia (Projects CTQ-2010-15364 and Project Consolider-Ingenio in Molecular Nanoscience, CSD2007-00010) and from the Generalitat Valenciana (PROMETEO Program).

ASSOCIATED CONTENT

Supporting Information

X-ray crystallographic data, in CIF format, IR spectra, Figures of electronic spectra and thermal analysis of complexes **1-3** are provided as supplementary material. This material is available free of charge via Internet at http://pubs.acs.org

AUTHOR INFORMATION

Corresponding Author

***E-mail**: scmanna@mail.vidyasagar.ac.in (S. C. Manna)

References

(1)(a) Batten, S. R.; Robson, R. *Angew. Chem., Int. Ed.***1998**, *37*, 1460–1494. (b) Eddaoudi, M.; Kim, J.; Rosi, N.; Vodak, D.; Wachter, J.; O'Keeffe, M.; Yaghi, O. M. *Science*, **2002**, *295*, 469–472. (c) O'Keeffe, M.; Peskov, M. A.; Ramsden, S. J.; Yaghi, O. M. *Acc. Chem. Res.***2008**, *41*, 1782–1789. (d) Perry IV, J. J.; Perman, J. A.; Zaworotko, M. J. *Chem. Soc. Rev.***2009**, *38*, 1400–1417. (e) Zeng, M. H.; Wang, Q. X.; Tan, Y. X.; Hu, S.; Zhao, H. X.; Long, L. S.; Kurmoo, M. *J. Am. Chem. Soc.***2010**, *132*, 2561–2563.

(2) (a) Sun, D.; Ma, S.; Ke, Y.; Collins, D. J.; Zhou, H. C. *J. Am. Chem. Soc.* **2006**, *128*, 3896-3897. (b) Eddaoudi, M.; Moler, D. B.; Li, H. L.; Chen, B. L.; Reineke, T. M.; O'Keeffe, M.; Yaghi, O. M. *Acc. Chem. Res.* **2001**, *34*, 319-330. (c) Yaghi, O. M.; O'Keeffe, M.; Ockwig, N. W.; Chae, H. K.; Eddaoudi, M.; Kim, J. *Nature*, **2003**, *423*, 705-714. (d) Férey, G.; Mellot-Draznieks, C.; Serre, C.; Millange, F. *Acc. Chem. Res.* **2005**, *38*, 217-225.

(3) (a) Latroche, M.; Surble, S.; Serre, C.; Mellot-Draznieks, C.; Llewellyn, P. L.; Lee, J. H.; Chang, J. S.; Jhung, S. H.; Ferey, G. *Angew. Chem., Int. Ed.* **2006**, *45*, 8227-8231. (b) Zeng, M. H.; Wang, B.; Wang, X. Y.; Zhang, W. X.; Chen, X. M.; Gao, S. *Inorg. Chem.* **2006**, *45*, 7069-7076. (c) Verbiest, T.; van Elshocht, S.; Karuanen, M.; Hellemans, L.; Snauwaert, J.; Nuckolls, C.; Katz, T. J.; Persoons, A. *Science* **1998**, *282*, 913-915.

(4) (a) Hagrman, P. J.; Hagrman, D.; Zubieta, J. *Angew. Chem., Int. Ed.***1999**, *38*, 2638-2684. (b) Chen, B.; Ma, S.; Zapata, F.; Fronczek, F. R.; Lobkovsky, E. B.; Zhou, H. C. *Inorg. Chem.* **2007**, *46*, 1233-1236. (c) Moulton, B.; Zaworotko, M. J. *Chem. Rev.* **2001**, *101*, 1629-1658.

(5) (a) Chen, B. L.; Ockwig, N. W.; Millward, A. R.; Contreras, D. S.; Yaghi, O. M. *Angew. Chem., Int. Ed.* **2005**, *44*, 4745-4749. (b) Kesanli, B.; Lin, W. *Coord. Chem. Rev.* **2003**,

246, 305-326. (c) Horike, S.; Matsuda, R.; Tanaka, D.; Mizuno, M.; Endo, K.; Kitagawa, S. *J. Am. Chem. Soc.* **2006**, *128*, 4222-4223.

(6) (a) Ma, L. F.; Wang, L. Y.; Huo, X. K.; Wang, Y. Y.; Fan, Y. T.; Wang, J. G.; Chen, S. H. *Cryst. Growth Des.* **2008**, *8*, 620-628. (b) Ma, L. F.; Wang, Y. Y.; Wang, L. Y.; Liu, J. Q.; Wu, Y. P.; Wang, J. G.; Shi, Q. Z.; Peng, S. M. *Eur. J. Inorg. Chem.* **2008**, 693-703.

(7) (a) Yang, J.; Yue, Q.; Li, G. D.; Cao, J. J.; Li, G. H.; Chen, J. S. *Inorg. Chem.* **2006**, *45*, 2857-2865. (b) Yue, Q.; Yang, J.; Li, G. H.; Li, G. D.; Xu, W.; Chen, J. S.; Wang, S. N. *Inorg. Chem.* **2005**, *44*, 5241-5246. (c) Ma, B. Q.; Zhang, D. S.; Gao, S.; Jin, T. Z.; Yan., C. H. *Angew. Chem., Int. Ed.* **2000**, *39*, 3644-3646.

(8) Yaghi, O. M.; Li, H. *J. Am. Chem. Soc.***1995**, *117*, 10401-10402.

(9) Gardner, G. B.; Venkataraman, D.; Moore, J. S.; Lee, S. *Nature*, **1995**, *374*, 792-795.

(10) (a) Gable, R.W.; Hoskins, B. F.; Robson, R. *J. Chem. Soc., Chem. Commun.***1990**, 1677-1678. (b) Fujita, M.; Kwon, Y. J.; Ashizu, S. W.; Ogura, K. *J. Am. Chem. Soc.*, **1994**, *116*, 1151-1152. (c) Hagrman, D.; Zubieta, C.; Rose, D. J.; Zubieta, J.; Haushalter, R. C. *Angew. Chem., Int. Ed. Engl.***1997**, *36*, 873-876.

(11) (a) Robinson, F.; Zaworotko, M. J. *J. Chem. Soc., Chem. Commun.***1995**, 2413-2414. (b) Yaghi, O. M.; Li, H. *J. Am. Chem. Soc.***1996**, *118*, 295-296.

(12) Fujita, M.; Kwon, Y. J.; Sasaki, Y. O.; Yamaguchi, K.; Ogura, K. *J. Am. Chem. Soc.***1995**, *117*, 7287-7288.

(13) (a) Losier, P.; Zaworotko, M. J. *Angew. Chem., Int. Ed. Engl.***1996**, *35*, 2779-2782. (b) Hennigar, T. L.; MacQuarrie, D. C.; Losier, P.; Rogers, R. D.; Zaworotko, M. J. *Angew. Chem., Int. Ed. Engl.***1997**, *36*, 972-973.

(14) (a) Soma, T.; Yuge, H.; Iwamoto, T. *Angew. Chem., Int. Ed. Engl.***1994**, *33*, 1665-1666. (b) Subramanian, S.; Zaworotko, M. J. *Angew. Chem., Int. Ed. Engl.* **1995**, *34*, 2127-2129.

(15) (a) Biradha, K.; Fujita, M. *Chem. Commun.* **2001**, 15-16. (b) Plater, M. J.; Foreman, M. R. S. J.; Gelbrich, T.; Coles, S. J.; Hursthouse, M. B. *J. Chem. Soc., Dalton Trans.* **2000**, 3065-3073.

(16) Kim, H.; Shu, M. P. *Inorg. Chem.* **2005**, *44*, 810-812.

(17) (a) http://www.chem.monash.edu.au/staff/sbatten/index.html, and references therein. (b) Carlucci, L.; Ciani, G.; Proserpio, D. M.; Rizzato, S. *Chem. Eur. J.* **2002**, *8*, 1519-1526. (c) Metrangolo, P.; Meyer, F.; Pilati,T.; Proserpio, D. M.; Resnati, G. *Chem. Eur. J.* **2007**, *13*, 5765-5772. (d) Batten, S. R.; Robson, R. *Angew. Chem., Int. Ed.* **1998**, *37*, 1460-1494. (e) Hsu, Y.-F.; Lin, C.-H.; Chen, J.-D.; Wang, J.-C. *Cryst. Growth Des.* **2008**, *8*, 1094-1096.

(18) (a) Manna, S. C.; Okamoto, K.; Zangrando, E.; Ray Chaudhuri, N. *CrystEngComm*, **2007**, *9*, 199–202. (b) Manna, S. C.; Konar, S.; Zangrando, E.; Okamoto, K. -i.; Ribas, J.; Ray Chaudhuri, N. *Eur. J. Inorg. Chem.*, **2005**, 4646–4654. (c) Manna, S. C.; Jana, A. D.; Rosair, G. M.; Drew, M. G. B.; Mostafa, G.; Ray Chaudhuri, N. *Journal of Solid State Chemistry*, **2008**, *181*, 457–466.

(19) (a) Bakalbassis, E. G.; Korabik, M.; Michailides, A.; Mrozinski, J.; Raptopoulou, C.; Skoulika, S.; Terzis, A.; Tsaousis, D. *J. Chem. Soc., Dalton Trans.* **2001**, 850-857. (b) Livage, C.; Egger, C.; Nogues, M.; Férey, G. *J. Mater. Chem.* **1998**, *8*, 2743-2747. (c) Livage, C.; Egger, C.; Férey, G. *Chem. Mater.* **1999**, *11*, 1546-1550. (d) Deakin, L.; Ariff, A. M.; Miller, J. S. *Inorg. Chem.* **1999**, *38*, 5072-5077. (e) Lo, M. -F. S.; Chui, S. -Y. S.; Willams, I. D.; Shek, L. Y.; Lin, Z.; Zang, X. X.; Wen, G. H. *J. Am. Chem. Soc.* **2000**, *122*, 6293-6294.

(20) (a) Manna, S. C.; Mistri, S.; Jana, A. D. *CrystEngComm* **2012**, *14*, 7415-7422. (b) Mistri, S.; Zangrando, E.; Manna, S. C. *Polyhedron*, **2013**, *49*, 252–258. (c) Mistri, S.; Zangrando, E.; Manna, S. C. *Inorganica Chimica Acta*, **2013**, *405*, 331–338. (d) Manna, S. C.; Zangrando, E.; Ribas, J.; Ray Chaudhuri, N. *Dalton Trans.***2007**, 1383-1391. (e) Manna, S. C.; Zangrando, E.; Ribas, J.; Ray Chaudhuri, N. *Eur. J. Inorg. Chem.* **2007**, 4592-4595. (f) Konar, S.; Manna, S. C.; Zangrando, E.; Mallah, T.; Ribas, J.; Ray Chaudhuri, N. *Eur. J. Inorg. Chem.* **2004**, 4202-4208. (g) Manna, S. C.; Zangrando, E.; Drew, M. G. B.; Ribas, J.; Ray Chaudhuri, N. *Eur. J. Inorg. Chem.* **2006**, 481-488. (h) Manna, S. C.; Zangrando, E.; Bencini, A.; Benelli, C.; Ray Chaudhuri, N. *Inorg. Chem.***2006**, *45*, 9114-9122.

(21) (a) Sun, Q.; Cheng, A. –l.; Wang, Y. –Q.; Ma, Y.; Gao, E. –Q. *Inorg. Chem.* **2011**, *50*, 8144–8152. (b) Fang, Q. –R.; Zhu, G. –S.; Xue, M.; Zhang, Q. –L.; Sun, J. –Y.; Guo, X. –D.; Qiu, S. –L.; Xu, S. –T.; Wang, P.; Wang, D. –J.; Wei, Y. *Chem. Eur. J.* **2006**, *12*, 3754 – 3758.

(22)(a) Armentano, D.; Mastropietro, T. F.; De Munno, G.; Rossi, P.; Lloret, F.; Julve, M. *Inorg. Chem.* **2008**, *47*, 3772-3786. (b) Sieklucka, B.; Podgajny, R.; Pinkowicz, D.; Nowicka, B.; Korzeniak, T.; Bałanda, M.; Wasiutyński, T.; Pełka, R.; Makarewicz, M.; Czapla, M.; Rams, M.; Gaweł, B.; Łasocha, W. *CrystEngComm*, **2009**, *11*, 2032–2039. (c) Tamaki, H.; Zhong, Z. J.; Matsumoto, N.; Kida, S.; Koikawa, M.; Achiwa, N.; Hashimoto, Y.; Okawa, H. *J. Am. Chem. Soc.* **1992**, *114*, 6974.

(23) (a) Zadrozny, J. M.; Long, J. R. *J. Am. Chem. Soc.* **2011**, *133*, 20732-20734. (b) Vallejo, J.; Castro, I.; Ruiz-García, R.; Cano, J.; Julve, M.; Lloret, F.; De Munno, G.; Wernsdorfer, W.; Pardo, E. *J. Am. Chem. Soc.* **2012**, *134*, 15704-15707. (c) Colacio, E.; Ruiz, J.; Ruiz,

E.; Cremades, E.; Krzystek, J.; Carretta, S.; Cano, J.; Guidi, T.; Wernsdorfer, W.; Brechin, E. K. *Angew. Chem. Int. Ed.* **2013**, *52*, 9130 -9134.

(24) Bruker, *SMART, SAINT. Software Reference Manual Bruker AXS Inc.* Madison, Wisconsin, USA, **2000**.

(25) Sheldrick, G. M. *Acta Cryst*. **2008**, *A64* , 112-122.

(26) Farrugia, L. J. *J. Appl. Crystallogr*. **1999**, *32*, 837-838.

(27) K. Nakamoto, Infrared Spectra of Inorganic and Coordination Compounds, John Wiley & Sons, New York, **1997**.

(28) A. B. P. Lever, Inorganic Electronic Spectroscopy, Elsevier Publishing Company, New York, **1968**.

(29) (a) Zhao, H.; Ye, Q.; Wu, Q.; Song, Y. -M.; Liu, Y. -J.; Xiong, R. -G. *Z. Anorg. Allg. Chem.* **2004**, *630*, 1367-1370. (b) Hui, PAN; Yan, BAI; Bing, AN; Dong-Bin, DANG *Chinese Journal of Inorganic Chemistry*, **2013**, *29*. (c) Hu, Z.; Pramanik, S.; Tan, K.; Zheng, C.; Liu, W.; Zhang, X.; Chabal, Y. J.; Li, J. *Cryst. Growth & Desgn*. **2013**, *13*, 4204-4217.

(30) Sun, Q.; Yue, Q.; Zhang, J. –Y.; Wang, L.; Li, X.; Gao, E. –Q. *Cryst. Growth Des.* **2009**, *9*, 2310-2317.

(31) (a) Ma, L. –F.; Wang, L. –Y.; Wang, Y. –Y.; Batten, S. R.; Wang, J. –G. *Inorg. Chem*. **2009**, *48*, 915-924. (b) Peedikakkal, A. M. P.; Song, Y. –M.; Xiong, R. –G.; Gao, S.; Vittal, J. J. *Eur. J. Inorg. Chem*. **2010**, 3856-3865. (c) Tao, J.; Tong, M. –L.; Chen, X. –M. *J. Chem. Soc., Dalton Trans*. **2000**, 3669-3674.

(32) Batten, S. R.; Robson, R. *Angew. Chem. Int. Ed.***1998**, *37*, 1460-1494.

(33) Tao, J.; Tong, M. –L.; Chen, X. –M. *J. Chem. Soc., Dalton Trans*. **2000**, 3669-3674.

(34) Spek, A. L. *Acta Crystallogr. Sect A*, **1990**, *C34*, 46.

(35) (a) Borràs-Almenar, J. J.; Clemente-Juan, J. M.; Coronado, E.; Tsukerblat, B. S. *J. Comput. Chem.* **2001**, 22, 985-991. (b) Borràs-Almenar, J. J.; Clement-Juan, J. M.; Coronado, E.; Tsukerblat, B. S. *Inorg. Chem.* **1999**, 38, 6081-6088.

(36) Lloret, F.; Julve, M.; Cano, J.; Ruiz-García, R.; Pardo, E. *Inorg. Chim. Acta*, **2008**, 3432-3445.

(37) Cano, VPMAG package version 2.2; University of Valencia, Valencia, Spain, **2003**.

(38) E. Colacio, H. Aouryaghal, A. J. Mota, J. Cano, Reijo Sillanpää, A. Rodríguez-Diéguez, *CrystEngComm* **2009**, *11*, 2054–2064; M. Sarkar, G. Aromí, ,J. Cano, V. Bertolasi, D. Ray, Chem. Eur. J., **2010**, *16*, 13825–1383.

(39) Colacio, E.; Ruiz, J.; Ruiz, E.; Cremades, E.; Krzystek, J.; Carreta, S.; Cano, J.; Guidi, T.; Wernsdorfer, W.; Brechin, E. K. *Angew. Chem. Int. Ed*. **2013**, *52*, 9130-9134.

(40) Vallejo, J.; Castro, I.; Ruiz-García, R.; Cano, J.; Julve, M.; Lloret, F.; De Munno, G.; Wernsdorfer, W.; Pardo, E. *J. Am. Chem. Soc*. **2012**, *134*, 15704-15707.

(41) Neilson, J. R.; Morse, D. E.; Melot, B. C.; Shoemaker, D. P.; Kurzman, J. A.; Seshadri, R. *Phys. Rev. B*, **2011**, *83*, 094418 and references therein.

Table 1. Crystal Data and Structure Refinement for compounds **1-3**.

	1	**2**	**3**
Empirical formula	$C_{72}H_{60}Mn_2N_8O_{14}$	$C_{22}H_{30}CoN_2O_{13}$	$C_{24}H_{21}CoN_2O_{4.50}$
Formula mass, g mol^{-1}	1371.16	589.41	468.36
Cryst system	Triclinic	Triclinic	Triclinic
Space group	$P\bar{1}$	$P\bar{1}$	$P\bar{1}$
a, Å	11.0242(3)	7.5539(9)	9.7210(10)
b, Å	12.0925(4)	8.4979(8)	10.9804(18)
c, Å	13.6836(4)	20.6375(12)	11.479(2)
α ,deg	83.092(2)	87.947(11)	97.966(10)
β, deg	69.4980(10)	83.923(10)	96.212(11)
γ, deg	68.645(2)	72.251(12)	98.244(13)
V, Å^3	1139.27(13)	254.6(2)	1190.6(3)
Z	1	2	2
$D_{(calcd)}$, g cm^{-3}	1.431	1.560	1.306
μ(Mo-Kα), mm^{-1}	0.472	0.756	0.753
F(000)	710	614	484
Theta range, deg	1.59 - 26.73	1.98 - 27.11	1.81 - 26.37
No. of collcd data	22886	19599	16898
No. of unique data	6540	5467	4810
R_{int}	0.0505	0.0239	0.0626
Obs reflections [$I > 2\sigma(I)$]	3845	4667	2886
Goodness of fit (F^2)	1.039	1.071	0.975
Parameters refined	451	376	360
$R1$ [$I > 2\sigma(I)$] [a]	0.0603	0.0355	0.0626
$wR2$ [$I > 2\sigma(I)$] [a]	0.1695	0.1066	0.1634
Residuals, e Å^{-3}	0.880, –0.807	0.910, –0.631	0.566, –0.468

[a] $R1(Fo) = \Sigma \big| |Fo| - |Fc| \big| / \Sigma |Fo|$, $wR2(Fo^2) = [\Sigma w (Fo^2 - Fc^2)^2 / \Sigma w (Fo^2)^2]^{1/2}$

Table 2. Coordination bond lengths (Å) and angles (°) for complexes **1**-**3**.

Complex **1**			
Mn(1)-O(1)	2.119(2)	Mn(1)-N(2)	2.295(3)
Mn(1)-O(1w)	2.126(2)	Mn(1)-N(3)	2.305(3)
Mn(1)-N(1)	2.303(3)	Mn(1)-N(4)	2.303(3)
O(1)-Mn-O(1w)	98.82(9)	O(1w)-Mn-N(4)	162.83(14)
O(1)-Mn-N(1)	94.81(10)	N(1)-Mn-N(3)	157.89(10)
O(1)-Mn-N(2)	166.72(12)	N(1)-Mn-N(2)	72.19(11)
O(1)-Mn-N(3)	99.47(10)	N(1)-Mn-N(4)	94.18(12)
O(1)-Mn-N(4)	80.06(9)	N(2)-Mn-N(3)	92.24(10)
O(1w)-Mn-N(1)	102.98(11)	N(2)-Mn-N(4)	97.82(10)
O(1w)-Mn-N(2)	87.04(9)	N(3)-Mn-N(4)	71.97(12)
O(1w)-Mn-N(3)	91.46(11)		
Complex **2** [a]			
Co(1)-O(1)	2.0903(14)	Co(2)-O(5)	2.0375(14)
Co(1)-O(3)	2.0796(13)	Co(2)-O(2w)	2.0897(15)
Co(1)-O(1w)	2.0945(14)	Co(2)-O(3w)	2.1564(18)
O(1)-Co(1)-O(3)	92.54(6)	O(5)-Co(2)-O(2w")	92.35(6)
O(1)-Co(1)-O(3')	87.46(6)	O(5)-Co(2)-O(2w)	87.65(6)
O(1)-Co(1)-O(1w)	90.78(6)	O(5)-Co(2)-O(3w)	86.79(7)
O(1)-Co(1)-O(1w')	89.22(6)	O(5)-Co(2)-O(3w")	93.21(7)
O(3)-Co(1)-O(1w)	90.17(6)	O(2w)-Co(2)-O(3w)	88.64(7)
O(3)-Co(1)-O(1w')	89.83(6)	O(2w)-Co(2)-O(3w")	91.36(7)
N(1)-O(1)-Co(1)	120.18(11)		
Complex **3**			
Co-O(1)	1.994(3)	Co-O(4)	2.201(3)
Co-O(2')	2.021(3)	Co-N(1)	2.165(3)
Co-O(3)	2.173(3)	Co-N(2")	2.152(4)
O(1)-Co-O(2')	110.89(13)	O(2')-Co-N(2")	94.58(14)
O(1)-Co-O(3)	154.69(15)	O(3)-Co-O(4)	59.16(14)

O(1)-Co-O(4)	96.13(14)	O(4)-Co-N(1)	88.81(14)
O(1)-Co-N(1)	88.53(13)	O(3)-Co-N(1)	85.76(13)
O(1)-Co-N(2")	91.20(14)	O(4)-Co-N(2")	88.48(15)
O(2')-Co-O(3)	93.56(14)	O(3)-Co-N(2")	93.33(15)
O(2')-Co-O(4)	152.70(14)	N(1)-Co-N(2")	177.23(14)
O(2')-Co-N(1)	88.09(13)		

[a] Both cobalt ions located on a centre of symmetry. Symmetry operations: **2**: (') -x, -y+1, -z+1; (") -x+2, -y-2, -z; **3**: (') -x+1, -y, -z+2; (") x-1, y-1, z.

Table 3. H bond parameters for complexes **1** and **2**.

D-H	d(D-H)	d(H..A)	<DHA	d(D..A)	A	Symmetry code
Complex **1**						
O1w-H1a	0.814	1.936	175.42	2.749	O4	x-1,y,z
O1w-H1b	0.842	1.816	168.49	2.647	O3	-x+1,-y+2,-z
O2w-H2a	1.112	1.712	160.78	2.786	O3w	
O2w-H2b	0.742	2.084	162.98	2.802	O4	-x+1,-y+1,-z
O3w-H3a	0.940	1.958	151.93	2.822	O2	-x,-y+1,-z
O3w-H3b	0.922	1.865	168.14	2.774	O2	
Complex **2**						
O1w-H1a	0.795	1.922	158.01	2.676	O4	
O1w-H1b	0.731	2.056	169.63	2.779	O4w	x-1,y,z
O2w-H2a	0.804	1.941	154.73	2.690	O6	-x+2,-y-2,-z
O2w-H2b	0.811	2.004	169.92	2.807	O2	x,y-1,z
O3w-H3a	0.839	2.000	169.69	2.829	O2	x+1,y-1,z
O3w-H3b	0.785	2.056	163.05	2.817	O6w	-x+1,-y-1,-z
O4w-H4a	0.853	1.941	170.09	2.785	O1	
O4w-H4b	0.934	1.959	154.89	2.832	O7w	x,y+1,z
O5w-H5b	0.900	1.945	173.29	2.840	O4	
O5w-H5a	0.799	2.139	165.44	2.919	O7w	-x,-y,-z+1
O6w-H6b	0.877	1.955	167.63	2.818	O6	x-1,y+1,z
O6w-H6a	0.779	2.100	169.07	2.869	O5w	
O7w-H7a	0.850	2.043	153.93	2.831	O3	
O7w-H7b	0.850	-	-	-	-	

Caption of the Figures

Figure 1. Solid-state emission spectra of complexes **1-3** at room temperature (λ_{ex} = 270 nm, for **1**; 275 nm for **2;** 300 nm for **3**).

Figure 2. Ortep drawing (40% probability ellipsoid) of the complex cation of **1**. (Mn' at –1–x, 1–y, 1–z).

Figure 3. The uncoordinated ppda ligands sandwiched by phen ligands of two symmetry related complexes in complex of **1**.

Figure 4. π-π stacking interactions among the phen ligands and the uncoordinated dppa anions (in black) in **1** (of coordinated dppa only carboxylate groups shown for clarity).

Figure 5. Detail of the 1D coordination polymer of complex **2**. Both the cobalt atoms are located on a centre of symmetry

Figure 6. The 2D structure parallel to the [102] planes formed by π-π stacking interactions and H-bonds among in complex **2**.

Figure 7. The centrosymmetric dinuclear node in the three-fold interpenetrated structure of **3**.Only one of disordered phenyl ring and pyridine N2 are shown for clarity.

Figure 8. Perspective views of the two-dimensional sheets of $[Co(ppda)]_2$in complex **3** of dimensions 19.704(3) x 14.745(2) Å. The picture shows the disorder of the bis-chelating ppda about centres of symmetry and water molecules H-bonded to the framework.

Figure 9. A single cuboidal unit in the α-polonium-related net in complex **3**.

Figure 10. The three-fold interpenetrating α-Po-related nets in the structure of complex **3**. The linear connections represent the –$(CH)_2$–Ph–$(CH)_2$– fragment of ppda anions and dotted lines the bis-pyridyl-ethane connections.

Figure 11. Thermal dependence of the $\chi_M T$ for complex **1**. Symbols represent experimental data while straight lines represent the simulations obtained from the parameters indicated in the main text.

Figure 12. Temperature dependence of $\chi_M T$ of **2**. The inset shows an enlargement in the lower temperatures region. Solid line is the best-fit curve (see text).

Figure 13. M vs. H/T plots for **2**. Solid lines are only eye-guides.

Figure 14. Temperature dependence of $\chi_M T$ of **3** at 10000 G (black), 5000 G (light blue), 100 G (red), and 50 G (blue). Solid lines are only eye-guides.

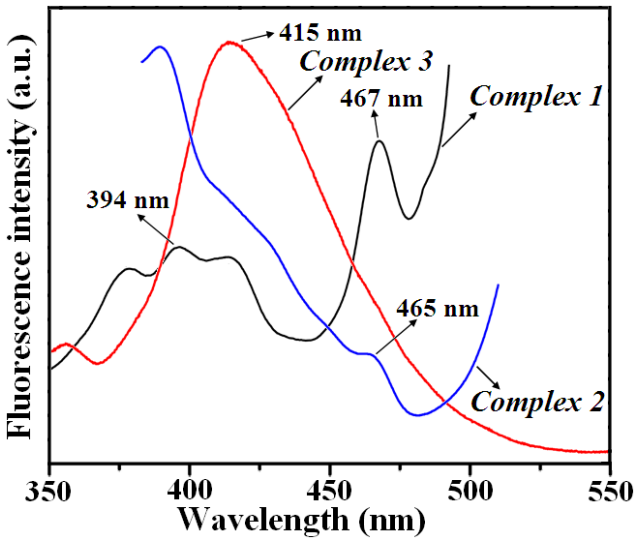

Figure 1

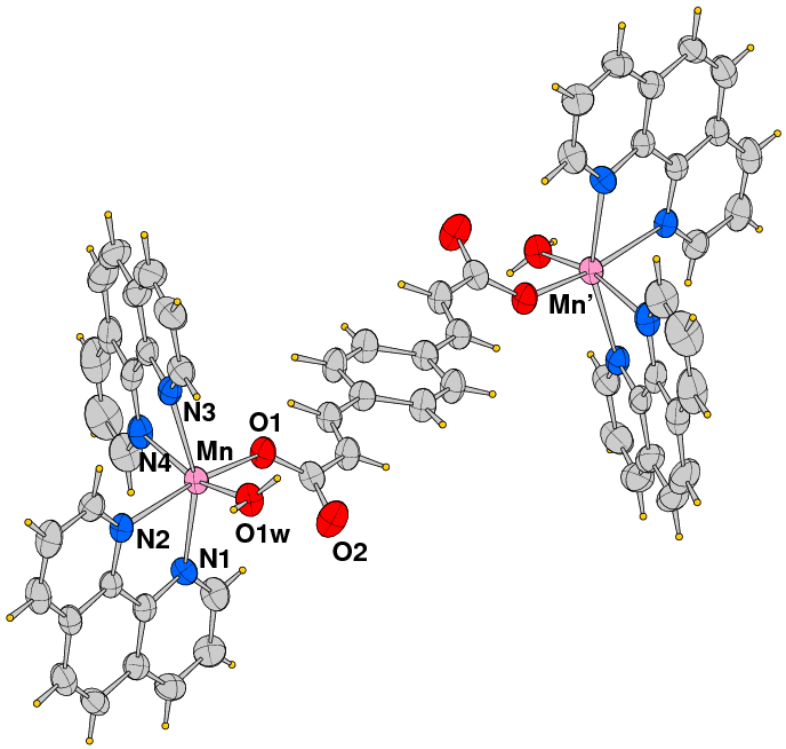

Figure 2

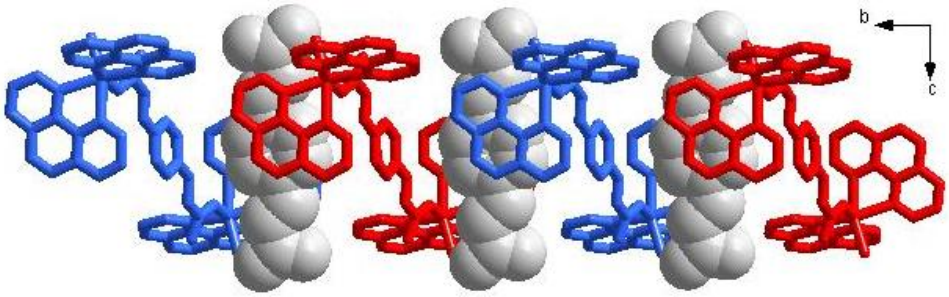

Figure 3

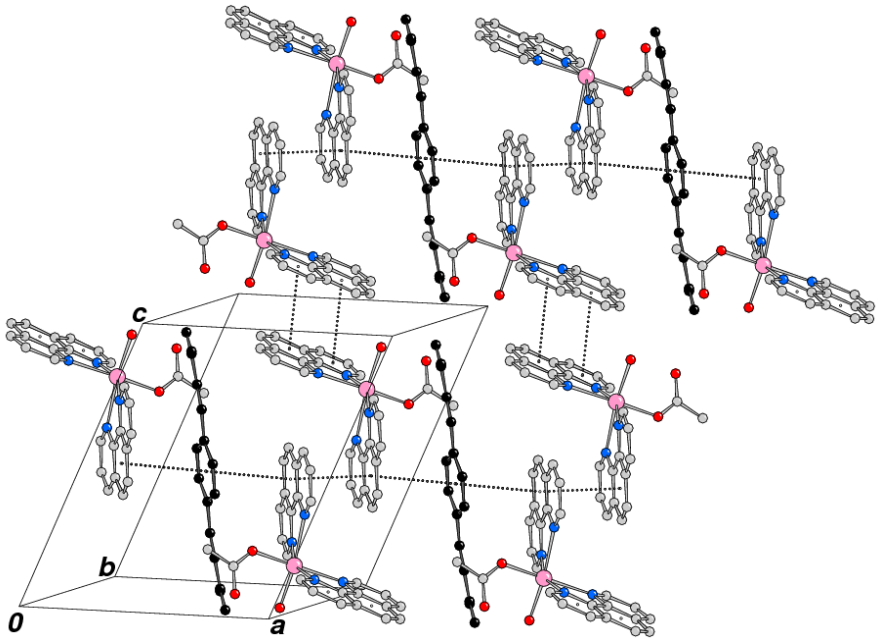

Figure 4

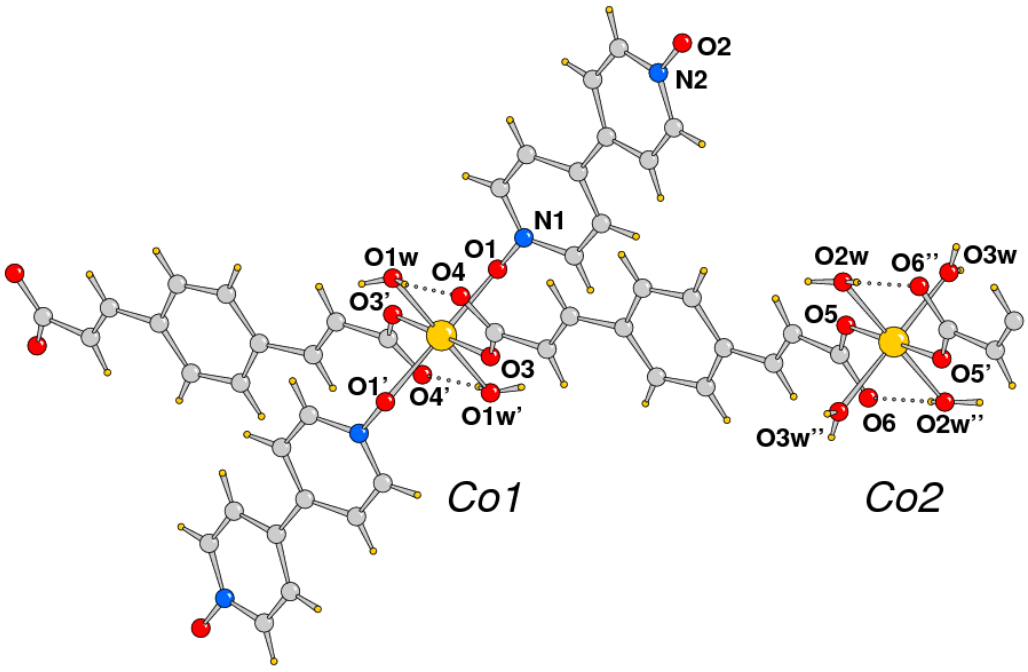

Figure 5

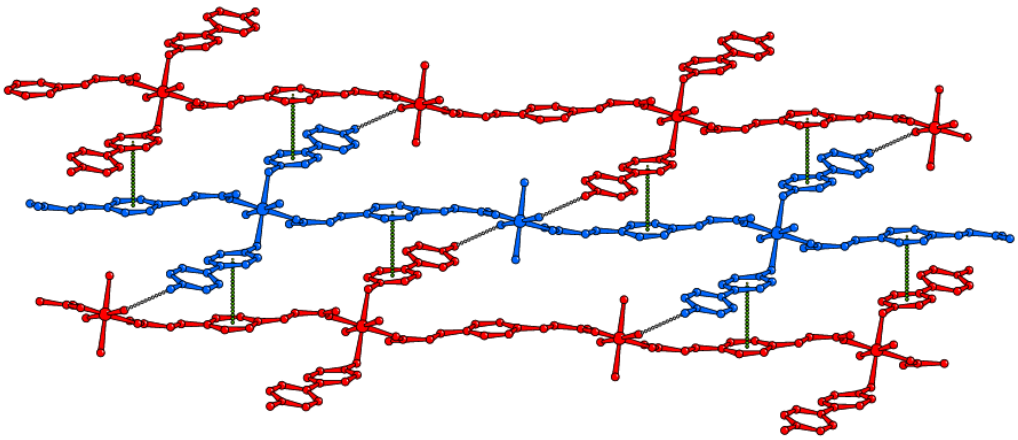

Figure 6

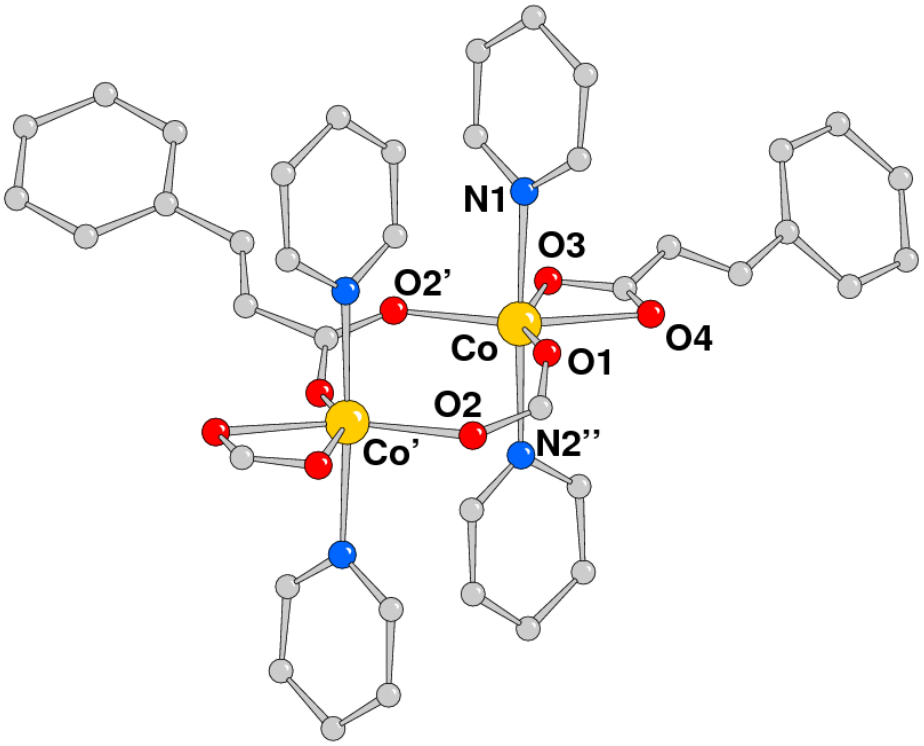

Figure 7

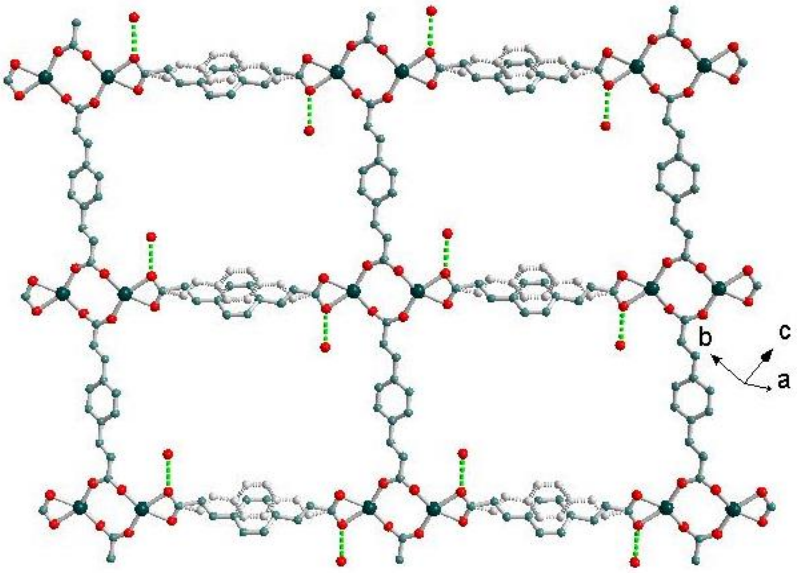

Figure 8

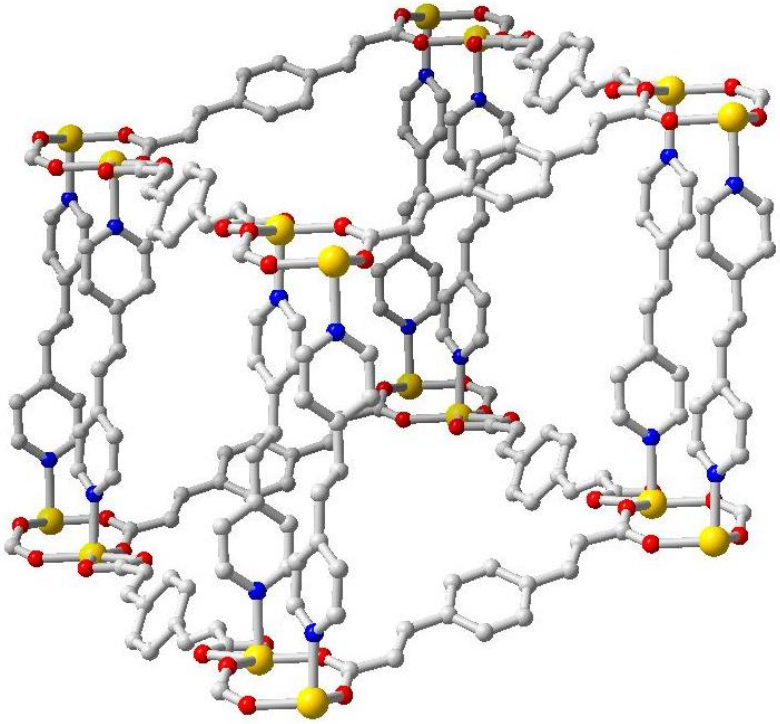

Figure 9

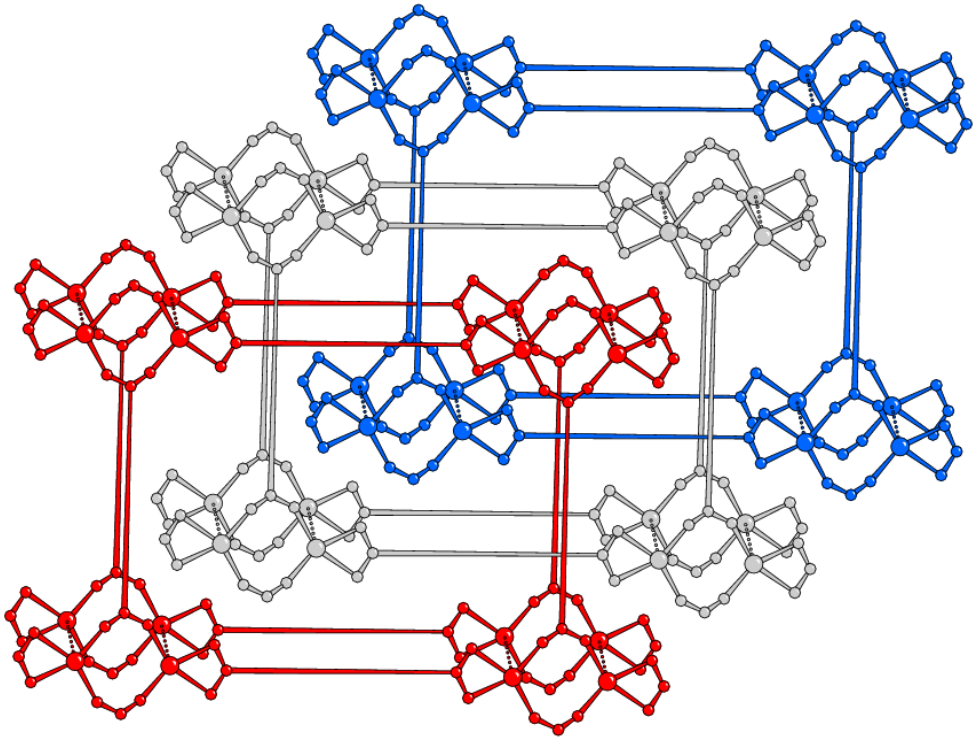

Figure 10

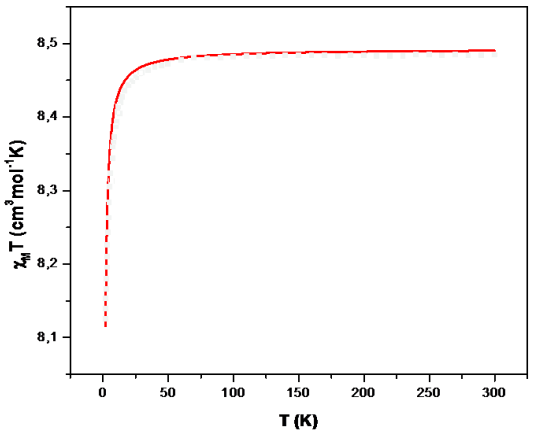

Figure 11

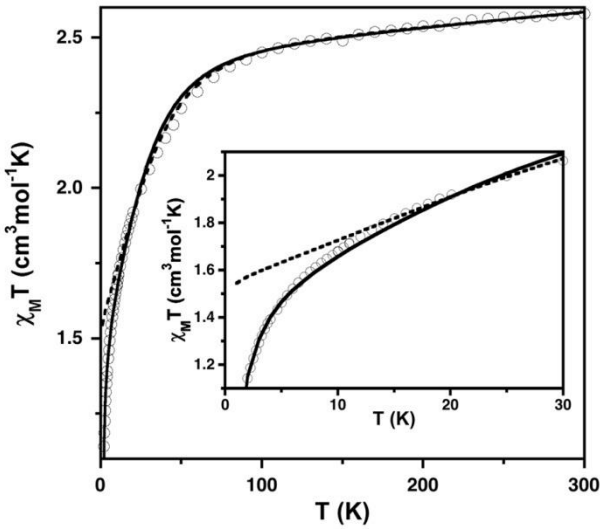

Figure 12

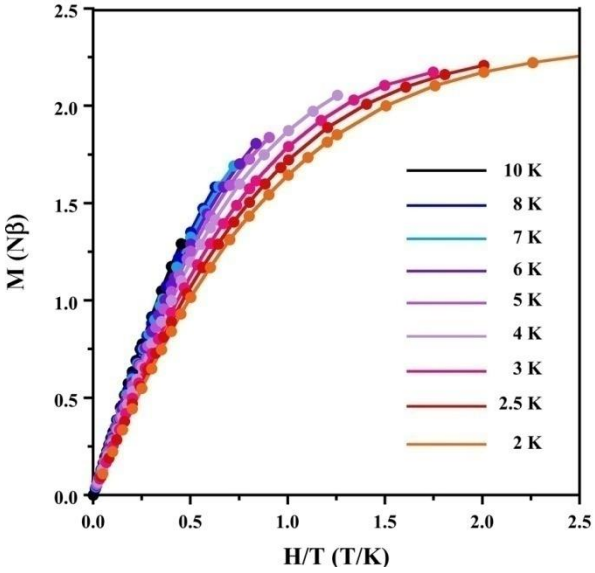

Figure 13

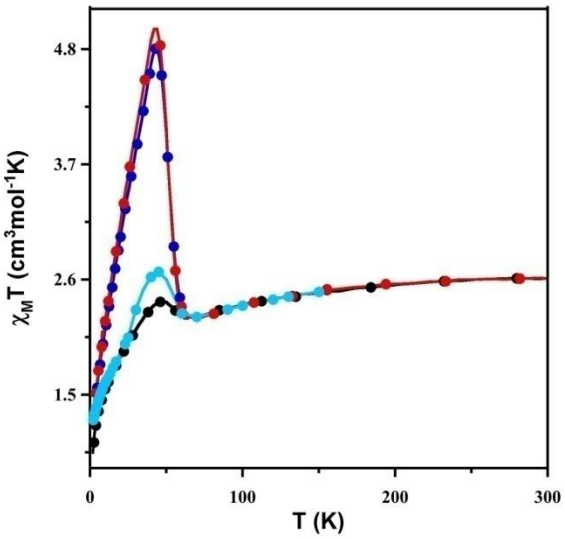

Figure 14

Content

Syntheses, Crystal Structures, and Magnetic Properties of Metal-Organic Hybrid Materials of Mn(II)/Co(II): Unprecedented 3D Three-fold Interpenetrated α-Polonium-like Network in One of Them

Soumen Mistri, Subal Chandra Manna, Ennio Zangrando, Albert Figuerola, Joan Cano, Amit Adhikary

Metal-organic hybrid materials, $\{[Mn_2(phen)_4(H_2O)_2(ppda)]\cdot(ppda)\cdot 2(H_2O)\}$(**1**), $\{[Co(ppda)(dpyo)(H_2O)_3]\cdot 4(H_2O)\}_n$ (**2**), and $\{[Co(ppda)(bpe)]\cdot(0.5H_2O)\}_n$ (**3**) [phen = 1,10-phenanthroline; ppda = 1,4-phenylenediacrylate; dpyo = 4,4´-dipyridyl *N*,*N*´-dioxide; bpe = 1,2-bis(4-pyridyl)ethane]have been synthesized and characterized by single-crystal X-ray diffraction analyses. Low-temperature magnetic measurements indicates antiferromagnetic coupling in all cases.